Material Classification of Multi-energy CT images Using Multiple Discriminant Analysis

Woo-Jin Lee, Dae-Seung Kim, Se-Ryong Kang, Sang-Yoon Woo, and Won-Jin Yi

Abstract—**Energy resolved photon-counting detectors could achieve more than one spectral measurement. The goal of this study is to investigate, with experiment, the ability to decompose five materials using energy discriminating detectors and multiple discriminant analysis (MDA). A small field-of-view multi-energy CT system was built. Linear attenuation coefficient was considered as features of multiple energy CT. MDA was used to decompose five materials with six measurements of the energy dependent linear attenuation coefficients. The results of the experimental study showed that a CT system based on CdTe detectors with MDA can be used to decompose five materials.**

I. Introduction

All materials has different linear attenuation coefficient depending on the X-ray energy [1]. Using these properties, materials could be discriminated in computed tomography (CT). There are two types of approaches to identify specific materials: one is in the projection domain (pre-reconstruction) [1, 2] and the other in the image domain (post-reconstruction) [3-5]. Although decomposition in the projection domain is beneficial to removing the beam hardening effect, the image domain is computationally more efficient. In this study, we adopted the image domain and assumed that each voxel consists of single material.

*This work was supported by the National Research Foundation of Korea (NRF) grant funded by the Korea government (MEST) (No. 2013R1A2A2A03067942)

Woo-jin Lee is with Interdisciplinary Program in Radiation Applied Life Science major, College of Medicine, Seoul National University, South Korea (e-mail: lwj0616@snu.ac.kr).

Dae-Seung Kim was with Interdisciplinary Program in Radiation Applied Life Science major, College of Medicine, Seoul National University, Seoul, South Korea. He is now with the Dental Research, Seoul National University, South Korea (e-mail: diers@snu.ac.kr).

Se-Ryong Kang is with Department of Biomedical Radiation Sciences, Graduate School of Convergence Science and Technology, Seoul National University, Seoul, South Korea (e-mail: seryongkang@snu.ac.kr).

Sang-yoon Woo is with Interdisciplinary Program in Radiation Applied Life Science major, College of Medicine, Seoul National University, South Korea (e-mail: woodli14@snu.ac.kr).

Won-jin Yi is with Department of Oral and Maxillofacial Radiology, School of Dentistry, Seoul National University, South Korea (corresponding author to provide phone: (+82)2-2072-3049; fax: (+82)2-744-3919; e-mail: wjyi@snu.ac.kr).

In order to acquire multi-energy X-ray images, the number of measurements should be equal or more than the number of materials. Due to the imperfections of detector technology, previous researches mostly focused on two measurements and two materials. Several methods such as sandwich detector and fast kV switching have been also utilized as well as the dual source methods [6, 7]. These techniques, thus, provide limited number of energy bins and energy resolution is inefficient.

According to the advance of technologies, photon counting method has been provided and it has several advantages; the most radiation-efficient, low-dose, and multi energy X-ray detecting [8]. Due to the usefulness of photon counting detector, this method has been conducted by many researchers [9-13]. As the previous researchers have shown, multi-energy can support to distinguish the materials by exploiting atomic reacting to various energy domains. Specifically, functional imaging that shows the characteristics of material component, not simply X-ray attenuation images, is feasible by using multi-energy X-ray images. Additionally, high Contrast-to-Noise ratio can be obtained with equal radiation dose.

To decompose the material, k-edge algorithm, least squares parameter estimation algorithm, and principal component analysis (PCA) algorithm have been implemented [13-15]. However, these algorithms have revealed some limitations to discriminate between materials. K-edge algorithm cannot be applied to materials which do not contain k-edge, and least squares estimation decomposition method is vulnerable to increased noise, especially in narrow energy bins of photon-counting detectors. Furthermore, while PCA algorithm have no consideration of any difference in class, multiple discriminant analysis (MDA) explicitly show the differences between the classes of data [16]. Nevertheless, both algorithms represent linear combinations of variables that best indicate the data.

978-1-4244-7929-0/14/$26.00 ©2014 IEEE

In this respect, this study aims to present methodology for the classification of the materials using MDA. A phantom study evaluating the technique's potential was performed discriminating up to five materials in the image domain using six energy bins and MDA.

II. Materials and Methods

A. Multi-energy CT System

We set up a prototype photon-counting CT system. The prototype device is presented in Figure 1. This system was made of a SourceRay SB-80–500 x-ray generator system (Source-Ray Inc., Bohemia, NY) capable of tube currents and voltages of 500 μA and 80 kVp, respectively. The x-ray source was operated at 500 μA and 80 kVp. The tube had a 40 μm focal spot size. All images were acquired through a CT system built with an energy resolving detector made of CdTe crystals. Medipix2 based CdTe detector (XRI-UNO, X-ray imatek, Spain) was used in photon counting mode. The energy ranges were set at 22-25, 26-29, 30-32, 33-36, 37-40, 41-44 keV.

The phantoms were rotated for 360, giving 320 frames per scan at 200 ms per frame. Photon counts for each energy were obtained with proprietary software (XRI-UNO GUI, X-ray imatek, Spain). All images were reconstructed with a FDK algorithm with the ramp filter [17]. Flat-field correction and ring artifact reduction method was performed on projection data [18].

Linear attenuation coefficient data acquired with the computed tomography from each energy bin E were transformed into spectral Hounsfield unit [19] as follows,

$$\mathrm{HU}_{E}(\mathrm{r}) = 1000 \times \frac{H_E^m(r) - H_E^{water}}{H_E^{water} - H_E^{air}}, \qquad (1)$$

where $H^m_E(\mathbf{r})$ is the linear attenuation coefficient of unknown material for each spatial coordinate $\mathbf{r}$, H^{water}_E is the linear attenuation coefficient of water, and H^{air}_E is the linear attenuation of air. Acryl was used as water equivalent material to calculate spectral HU.

B. Multiple Discriminant Analysis

We considered spectral HU of material as six-dimensional feature vector. Then we utilized the feature vector to classify the material using MDA algorithm. Let $\mathbf{x}^i_j$ be a d-dimensional column vector that denotes the jth sample from the ith class, and then $X = \{\mathbf{x}^1_1, \mathbf{x}^1_2, ..., \mathbf{x}^1_{N_1}, \mathbf{x}^2_1, ..., \mathbf{x}^C_{N_C}\}$ contains all the training samples. Then we can present as linear transform as follows,

$$\mathrm{y} = \mathbf{W}^{\mathrm{T}}\mathbf{x}, \qquad (2)$$

where $\mathbf{x}$ is sample vector and $\mathbf{W}$ is linear projection matrix.

Then intra-class covariance matrix for the number of class, c, is as follows,

$$S_W = \sum_{i=1}^{c} S_i ,$$

$$S_i = \sum_{\mathrm{x}\in\omega_i} (\mathrm{x} - \mu_{\mathrm{i}})(\mathrm{x} - \mu_{\mathrm{i}})^{\mathrm{T}}, \quad \mu_{\mathrm{i}} = \frac{1}{N_i}\sum_{\mathrm{x}\in\omega_i} \mathrm{x} . \qquad (3)$$

Then the inter-class covariance matrix is as follows,

$$S_B = \sum_{i=1}^{c} N_i(\mu_{\mathrm{i}} - \mu)(\mu_{\mathrm{i}} - \mu)^{\mathrm{T}}$$
$$\mu = \frac{1}{N}\sum_{\forall \mathrm{x}}^{\mathrm{c}} \mathrm{x} = \frac{1}{N}\sum_{\mathrm{x}\in\omega_i} N_i\mu_{\mathrm{i}} . \qquad (4)$$

Figure 1. Multi-energy CT experimental system with the detector on the left, the rotational stage in the middle, and x-ray tube on the right.

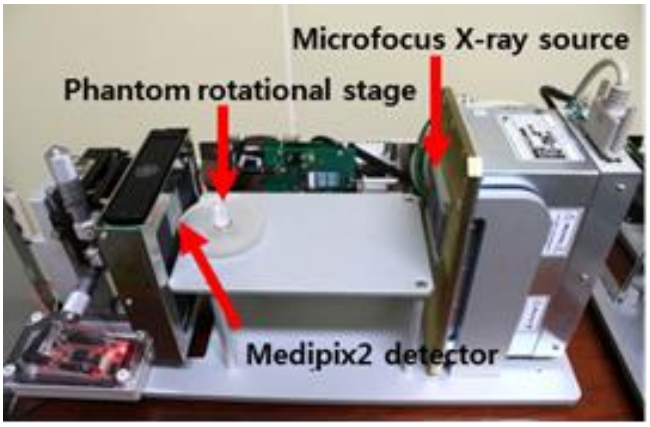

In order to separate the classes, we found a projection $\mathbf{W}$ that maximizes the following ratio:

$$J(W) = \frac{\left|W^T S_B W\right|}{\left|W^T S_W W\right|} . \qquad (5)$$

Optimal projection matrix W^* maximize the inter-class variation and minimize the intra-class variation. The projection matrix W^* was initially calculated from known material sample. Finally, discrimination was performed by comparing Euclidian distance.

C. Phantom

We fabricated a cylindrical acryl phantom with a 1 cm diameter circular cross section (Fig. 2). Inside the phantom, the left top contained bone-equivalent solution of $CaCl_2$(Calcium chloride), the right top contained gold nanoparticle (15 mg/ml), the bottom rows of contrast wells contained iodine solution (18.5 mg/ml and 37 mg/ml), respectively.

Figure 2. Transverse slice of the phantom scheme with calcium chloride, gold, iodine, and acryl cylinder.

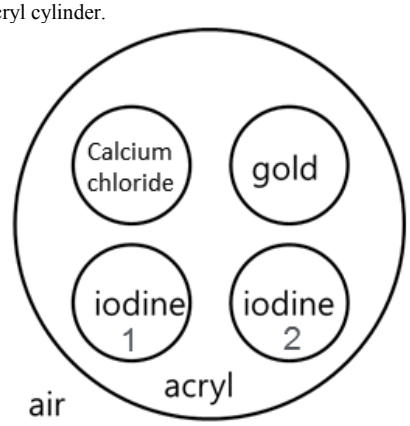

D. Data analysis and comparison

The two methods of material discrimination—MDA and Calibrated least squares fitting method (CLSF) [15]—were evaluated by comparing the results to both the ground truth and one another. The evaluation was performed by computing a metric that compares the decomposed region to the ground truth region from the phantom. The metric (O) can be computed as follows,

$$O = \frac{area\ (T \cap G)}{area\ (T \cup G)}, \tag{6}$$

where T is the image of a decomposed image and G is the ground truth image.

III. Results and Discussion

Reconstructed images of the phantom (Fig. 3) showed the tendency of attenuation coefficient regarding to energy bins. As revealed in Figure 3, higher energy bins 4, 5, and 6 had more artifacts caused by poor detector efficiency and low photon flux. Ring artifacts were present toward the center of the reconstructed images. This effect was more conspicuous in some energy bins than others: Energy bins 4, 5, and 6 had more ring artifacts than bins 1, 2, and 3.

Figure 4 displays graphs of measured HUs for iodine, calcium chloride, air, acryl and gold. Remarkably, as can be seen in this figure, the HU of calcium chloride and gold gradually decreased as expected while the photon energy increased, but around the k-edge of iodine (bin 3-4), HU of iodine was slightly risen.

In order to scrutinize the results of discrimination, the decomposed images for the MDA method are shown in figure 5. As this method produced material images which have a binary property, these images directly showed the result of the assumption that each voxel contains predominantly one material. In addition, the material separation algorithm implemented properly, whereas some voxels of gold were not separated correctly. The discrimination of iodine was found to be more precise than calcium chloride, as the k-edge of iodine more accurately identifies the materials within the measured energy range.

The values for the metric (O) are shown in Table 1. As shown in this table, the discrimination results are revealed that MDA is superior to CLSF in all different materials.

Figure 3. Transverse slices of the phantom for energy bins (a) 1, (b) 2, (c) 3, (d) 4, (e) 5, (f) 6.

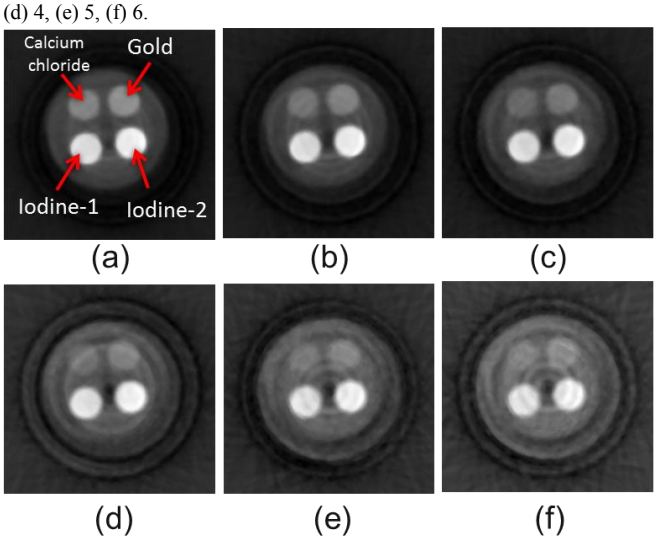

Figure 4. Spectral HU measurements for different substances across the images at different energy bin

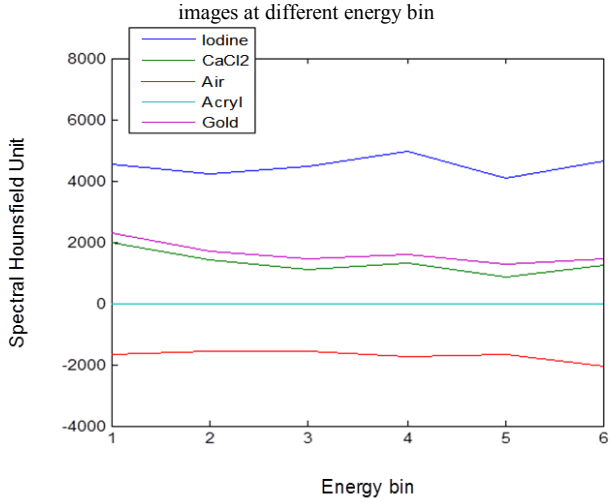

Figure 5. Decomposed images of calcium chloride (a), gold (b), iodine (c), acryl (d), and air (e) using the MDA algorithm.

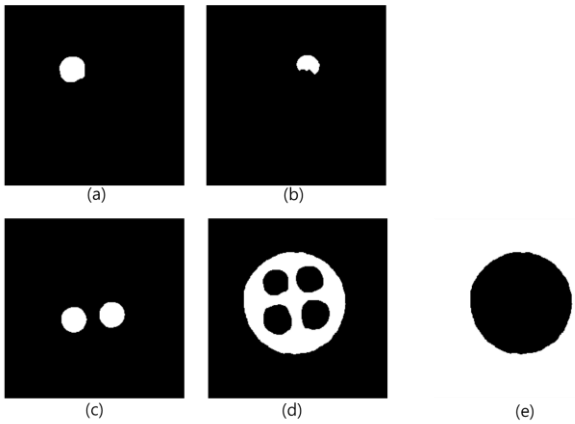

TABLE I. THE VALUES FOR *O* TO EVALUATE DISCRIMINATION RESULTS.

	Calcium chloride	**Gold**	**Iodine**	**Acryl**	**Air**
MDA	0.857	0.717	0.916	0.845	0.924
CLSF	0.674	0.703	0.775	0.831	0.836

IV. CONCLUSION

We developed multi-energy CT system using photon counting detector. We studied the problem of linear dimensionality reduction of the linear attenuation coefficient for the task of material classification. The results of the experimental study showed that a CT system based on CdTe detector with MDA can be used to decompose materials. For further research, novel ways of analyzing and observing data beyond Hounsfield Units will be needed.

REFERENCES

[1] R. E. Alvarez and A. Macovski, "Energy-Selective Reconstructions in X-Ray Computerized Tomography," *Physics in Medicine and Biology,* vol. 21, pp. 733-744, 1976.

[2] L. Yu, X. Liu, and C. H. McCollough, "Pre-reconstruction three-material decomposition in dual-energy CT," in *SPIE Medical Imaging*, 2009, pp. 72583V-72583V-8.

[3] P. V. Granton, S. I. Pollmann, N. L. Ford, M. Drangova, and D. W. Holdsworth, "Implementation of dual- and triple-energy cone-beam micro-CT for postreconstruction material decomposition," *Med Phys,* vol. 35, pp. 5030-42, Nov 2008.

[4] P. R. Mendonça, R. Bhotika, M. Maddah, B. Thomsen, S. Dutta, P. E. Licato*, et al.*, "Multi-material decomposition of spectral CT images," in *SPIE Medical Imaging*, 2010, pp. 76221W-76221W-9.

[5] Y. Yang, A. Tulloh, I. Cole, S. Furman, and A. Hughes, "A data-constrained computational model for morphology structures," *Journal of the Australasian Ceramic Society,* vol. 43, pp. 159-164, 2007.

[6] X. W. Wang, J. M. Li, K. J. Kang, C. X. Tang, L. Mang, Z. Q. Chen*, et al.*, "Material discrimination by high-energy x-ray dual-energy imaging," *High Energy Physics and Nuclear Physics-Chinese Edition,* vol. 31, pp. 1076-1081, Nov 2007.

[7] K. V. Haderslev and M. Staun, "Comparison of dual-energy x-ray absorptiometry to four other methods to determine body composition in underweight patients with chronic gastrointestinal disease," *Metabolism-Clinical and Experimental,* vol. 49, pp. 360-366, Mar 2000.

[8] X. Wang, D. Meier, K. Taguchi, D. J. Wagenaar, B. E. Patt, and E. C. Frey, "Material separation in x-ray CT with energy resolved photon-counting detectors," *Med Phys,* vol. 38, pp. 1534-46, Mar 2011.

[9] E. Beuville, R. Cahn, B. Cederstrom, M. Danielsson, A. Hall, B. Hasegawa*, et al.*, "High resolution X-ray imaging using a silicon strip detector," *Ieee Transactions on Nuclear Science,* vol. 45, pp. 3059-3063, Dec 1998.

[10] A. Breskin, "Advances in gas avalanche radiation detectors for biomedical applications," *Nuclear Instruments & Methods in Physics Research Section a-Accelerators Spectrometers Detectors and Associated Equipment,* vol. 454, pp. 26-39, Nov 1 2000.

[11] P. M. Shikhaliev, T. Xu, H. Le, and S. Molloi, "Scanning-slit photon counting x-ray imaging system using a microchannel plate detector," *Med Phys,* vol. 31, pp. 1061-71, May 2004.

[12] C. Szeles, S. A. Soldner, S. Vydrin, J. Graves, and D. S. Bale, "Ultra high flux 2-D CdZnTe monolithic detector Arrays for x-ray imaging applications," *Ieee Transactions on Nuclear Science,* vol. 54, pp. 1350-1358, Aug 2007.

[13] J. P. Schlomka, E. Roessl, R. Dorscheid, S. Dill, G. Martens, T. Istel*, et al.*, "Experimental feasibility of multi-energy photon-counting K-edge imaging in pre-clinical computed tomography," *Physics in Medicine and Biology,* vol. 53, pp. 4031-4047, Aug 7 2008.

[14] N. G. Anderson, A. P. Butler, N. J. Scott, N. J. Cook, J. S. Butzer, N. Schleich*, et al.*, "Spectroscopic (multi-energy) CT distinguishes iodine and barium contrast material in MICE," *Eur Radiol,* vol. 20, pp. 2126-34, Sep 2010.

[15] Q. Le Huy and S. Molloi, "Least squares parameter estimation methods for material decomposition with energy discriminating detectors," *Med Phys,* vol. 38, pp. 245-55, Jan 2011.

[16] R. O. Duda, P. E. Hart, and D. G. Stork, *Pattern classification*: John Wiley & Sons, 2012.

[17] L. A. Feldkamp, L. C. Davis, and J. W. Kress, "Practical Cone-Beam Algorithm," *Journal of the Optical Society of America a-Optics Image Science and Vision,* vol. 1, pp. 612-619, 1984.

[18] M. Yousuf and M. Asaduzzaman, "An efficient ring artifact reduction method based on projection data for micro-CT images," *Journal of Scientific Research,* vol. 2, pp. 37-45, 2009.

[19] M. A. Hurrell, A. P. Butler, N. J. Cook, P. H. Butler, J. P. Ronaldson, and R. Zainon, "Spectral Hounsfield units: a new radiological concept," *Eur Radiol,* vol. 22, pp. 1008-13, May 2012.